*International Journal of Remote Sensing*
Vol. 26, No. 8, 20 April 2005, 1575–1588

Taylor & Francis
Taylor & Francis Group

# A comparison of local variance, fractal dimension, and Moran's *I* as aids to multispectral image classification

CHARLES W. EMERSON†, NINA SIU-NGAN LAM‡ and DALE A. QUATTROCHI§

†Department of Geography, Western Michigan University, Kalamazoo, MI 49008-5053, USA; phone: 269-387-3430; fax: 269-387-3442; e-mail: charles.emerson@wmich.edu
‡Department of Geography and Anthropology, Louisiana State University, Baton Rouge, LA 70803, USA; phone: 225-578-6197; fax: 225-578-4420; e-mail: nlam@lsu.edu
§National Aeronautics and Space Administration, Earth Science Department, SD60, Marshall Space Flight Center, AL 35812, USA; phone: 256-961-7887; fax: 256-961-7788; e-mail: dale.quattrochi@ nasa.gov

(*Received 22 September 2003; in final form 23 September 2004*)

The accuracy of traditional multispectral maximum-likelihood image classification is limited by the multi-modal statistical distributions of digital numbers from the complex, heterogenous mixture of land cover types in urban areas. This work examines the utility of local variance, fractal dimension and Moran's *I* index of spatial autocorrelation in segmenting multispectral satellite imagery with the goal of improving urban land cover classification accuracy. Tools available in the ERDAS Imagine$^{TM}$ software package and the Image Characterization and Modeling System (ICAMS) were used to analyse Landsat ETM+ imagery of Atlanta, Georgia. Images were created from the ETM+ panchromatic band using the three texture indices. These texture images were added to the stack of multispectral bands and classified using a supervised, maximum likelihood technique. Although each texture band improved the classification accuracy over a multispectral only effort, the addition of fractal dimension measures is particularly effective at resolving land cover classes within urbanized areas, as compared to per-pixel spectral classification techniques.

## 1. Introduction

The synoptic view afforded by satellite imagery makes this data a potentially valuable resource for regional assessments of the biophysical impacts of urban sprawl. However, traditional multispectral image classification techniques have proven to be ineffective at identifying built-up areas (particularly at the urban-rural fringe), due to the heterogeneity of urban land covers (Johnsson 1994). The multi-modal statistical distributions of land cover types at the urban fringe limits the effectiveness of traditional multispectral maximum-likelihood classifiers, since suburban residential areas form a complex mosaic of trees, lawns, roofs, concrete driveways, and asphalt roadways. These details are imaged as mixed pixels by older, lower resolution sensors such as the Landsat Multispectral Scanner (MSS), whereas in newer, high-resolution commercial satellite imagery, urban areas form a complex surface of brightness values that could be viewed as a more detailed subset of the traditional notion of land cover.

Analytical techniques in remote sensing that explicitly consider the spatial structure of imaged features have primarily been measures of image texture (Chen

*International Journal of Remote Sensing*
ISSN 0143-1161 print/ISSN 1366-5901 online 
http://www.tandf.co.uk/journals
DOI: 10.1080/01431160512331326765

and Chen 1999). Grey-tone spatial-dependence or co-occurrence matrices (Haralick *et al*. 1973) provide the basis for a number of measures including range, variance, standard deviation, entropy, or uniformity within a moving window. These measures have been shown (Sali and Wolfson 1992, Carr and Miranda 1998) to be a potentially useful means for image classification. Zhang (1999) and Karathanassi *et al*. (2000) have evaluated the utility of co-occurrence matrices in urban land cover classification and have found that including textural information with spectral data generally improves classification accuracy. This work examines the utility of local variance, fractal dimension, and Moran's *I* index of spatial autocorrelation in segmenting Landsat 7 Enhanced Thematic Mapper multispectral imagery. The effectiveness of these indices were evaluated as additional layers in a supervised, maximum-likelihood image classification. Tools available in the ERDAS Imagine software package and the Image Characterization and Modeling System (ICAMS) (Quattrochi *et al*. 1997) were used to compute these local indices of texture.

## 2. Methods

### 2.1 *Study area*

Atlanta, Georgia, located in the southeastern United States (figure 1), is growing rapidly, both in terms of population and urbanized area. In the period from 1970 to 2000, Atlanta's population grew 133%, from approximately 1.8 million to over 4.1 million residents. Kolankiewicz and Beck (2001) found that Atlanta's urban area grew by 1817 square kilometres from 1970 to 1990, not only due to the increase in population, but also due to land use decisions that determine per capita land consumption. With few natural or anthropogenic barriers to continued growth, Atlanta is poised to spread well beyond its present urbanized area. Satellite remote sensing provides a unique viewpoint to track this explosive growth.

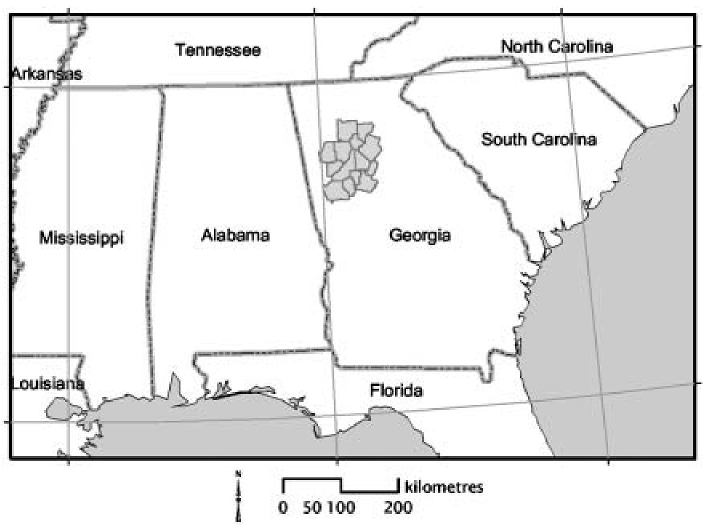


Figure 1. Location map of the southeastern United States showing Atlanta Regional Commission 13-county landcover study area.

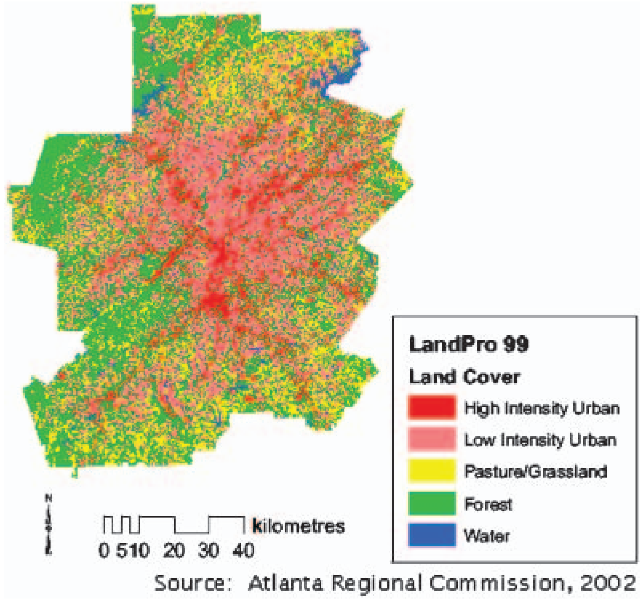


Figure 2. Land cover map of the Atlanta, Georgia area.

### 2.2 *Software*

The Image Characterization and Modeling System (ICAMS) is an integrated software package designed to provide specialized spatial analytical functions for visualizing and interpreting remote sensing data. The main functions contained in the ICAMS package include: fractal, variogram, spatial autocorrelation, wavelet and texture analysis. In its original form, ICAMS runs as an extension to the Intergraph-MGE and the Arc/Info Unix and Windows applications (Quattrochi *et al*. 1997, Lam *et al*. 1998). A stand alone C++ based Windows application and a multi-platform Java version also incorporate the fractal, wavelet, spatial autocorrelation, and other analytical functions (Zhao 2001). ICAMS can compute fractal dimension and spatial autocorrelation indices either in a global (whole image or major subset) or local fashion using a moving window filter.

The image file format conversions, georectifications, image classification, and accuracy assessment procedures used in this analysis were performed with the ERDAS Imagine™ version 8.6 (Leica 2002) image processing software package.

### 2.3 *Data types and sources*

Landsat 7 Enhanced Thematic Mapper (ETM+) panchromatic and multispectral images from October 28, 1999 were used in this study. Two adjacent scenes were mosaiced to create an image that included the Atlanta metropolitan area and surrounding countryside. The $4168 \times 5001$ pixel multispectral image included the six visible and reflective infrared bands. The $8351 \times 10017$ pixel panchromatic image was analysed using local variance, fractal dimension, and Moran's $I$ indices. The slightly larger spatial extent of the panchromatic image allowed moving window computations of texture throughout the entire area covered by the multispectral image. The panchromatic and multispectral Landsat images used in this analysis were registered to base map data (described in the accuracy assessment subsection) in Universal Transverse Mercator Zone 16 North coordinates using a second order polynomial model with nearest neighbour resampling.

### 2.4 *Indices of spatial complexity*

**2.4.1 Local variance.** A simple index of spatial complexity is the variance of grey scale values measured in a moving window. Most image analysis software packages include this method as a texture measure, with window sizes ranging from $3\times3$ up to $7\times7$ or larger. In this method, the real number representing the variance of the pixel values within the window is recorded for the window's central pixel location, the window steps over a predefined number of pixels and the variance of this window is recorded in the next pixel location. Woodcock and Strahler (1987) plotted local variance versus pixel sizes for an original image and several lower resolution, degraded versions of the original. These plots revealed the spatial structure of forested, urban, and other uniform scenes, and provided insights on the optimal resolution and image scale needed to analyse certain types of land covers.

**2.4.2 Fractal dimension.** Fractal analysis (Mandelbrot, 1983) provides tools for measuring the geometric complexity of imaged objects. In Euclidean space, a point has an integer topological dimension of zero, a line is one-dimensional (1D), an area has two dimensions and a volume three. The fractal dimension ($D$), however, is a non-integer value that, in Mandelbrot's (1983) definition for fractals, exceeds the topological dimension as the form of a point pattern, a line, or an area feature grows more geometrically complex. The fractal dimension of a point pattern can be any value between zero and one, a curve, between one and two, and a surface, between two and three. Increasing the geometrical complexity of a perfectly flat 2D surface ($D=2.0$) so that the surface begins to fill a volume, results in $D$ values approaching 3.0. Fractal techniques have been used to analyse the form and function of cities (Batty and Longley 1994), and have been an active area of research in machine vision (Pentland 1984; Chen *et al.* 1997).

There are many ways of computing the fractal dimension of a raster dataset, including the isarithm or walking-divider method, the triangular prism method, box-counting, and methods using semi-variograms (Quattrochi *et al.* 1997). This work uses the triangular prism method (Clarke 1986, Jaggi *et al.* 1993, Lam and DeCola 1993) as modified by Lam *et al.* (2002). This method constructs triangles by averaging the $z$-values (which in this case are the digital numbers) for sets of four adjacent pixels. The $z$-values for each pixel are used to establish heights at each corner, and triangles are formed by connecting these corner values to the height representing the mean value of the four pixels at the centre of the array (figure 3). Figure 4(*a*) shows an example $7\times7$ array of pixel values. In step 1 (figure 4(*b*)), the areas of all triangles at the tops of prisms consisting of $2\times2$ arrays of pixels are computed. The areas of the triangular 'facets' of the prisms are then summed to represent the total step 1 surface area. The algorithm then steps to $3\times3$ prisms (figure 4(*c*)), with the centre height corresponding to the average digital number at the four corners. The algorithm continues to increase the pixel size and compute the triangular prism areas until the entire surface is calculated as a single composite prism. The logarithm of the total of all the prism facet areas at each step is plotted against the logarithm of the prism dimension at each step. The fractal dimension is calculated by performing a least squares regression on these plotted points. The regression slope $B$ is used to determine the fractal dimension $D$, where $D=2–B$.

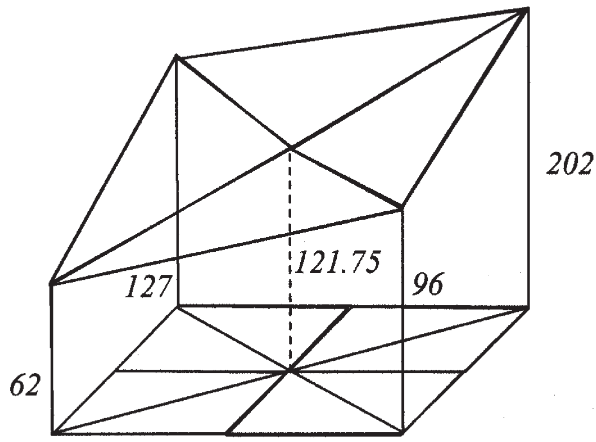


Figure 3. Construction of a triangular prism.

Noisy images with a 'rough' texture have widely different grey scale values closely adjacent and the amount of generalization that occurs as the facets get bigger is great, so that the slope of the log (prism facet area)/log (prism dimension) is steeply negative and the *D* value approaches 3.0. Smooth images have grey scale values that change slowly with distance, so the prism facet areas change relatively less with increasing prism dimension, the slope of the regression is near zero, and the *D* value approaches 2.0.

**2.4.3 Moran's I.** Spatial autocorrelation of raster images can be characterized by statistics such as Moran's *I* (Cliff and Ord 1973), which reflect the differing spatial structures of the smooth and rough surfaces. Moran's *I* is calculated from the following formula:

$$I(d) = \frac{n \sum_{i}^{n} \sum_{j}^{n} w_{ij}(z_i - \bar{z})(z_j - \bar{z})}{W \sum_{i}^{n} (z_i - \bar{z})^2} \tag{1}$$

where $w_{ij}$ is the weight at distance $d$, so that $w_{ij} = 1$ if point $j$ is within distance $d$ from point $i$, otherwise $w_{ij} = 0$ (rook's case adjacencies were assumed in the algorithm used here, limiting comparisons to pixels that share an edge). The $z$'s are pixel digital numbers, and $W$ is the sum of all the weights where $i \neq j$. As shown in figure 5, Moran's $I$ varies from $+1.0$ for perfect positive correlation (a clumped pattern) to 0.0 for a random pattern, to $-1.0$ for perfect negative correlation (a chequerboard pattern) (Goodchild 1980).

### 2.5 *Texture analysis*

In this example, texture images were computed from the 15 m spatial resolution Landsat ETM+ panchromatic band using a $21 \times 21$ pixel moving window incremented by two pixels at each step of the window. When the window reached the last position at which the entire window could be evaluated, the window skipped a row and started at the beginning of the following row in the image. This two-pixel increment between rows and columns produced a 30 m resolution texture image. The

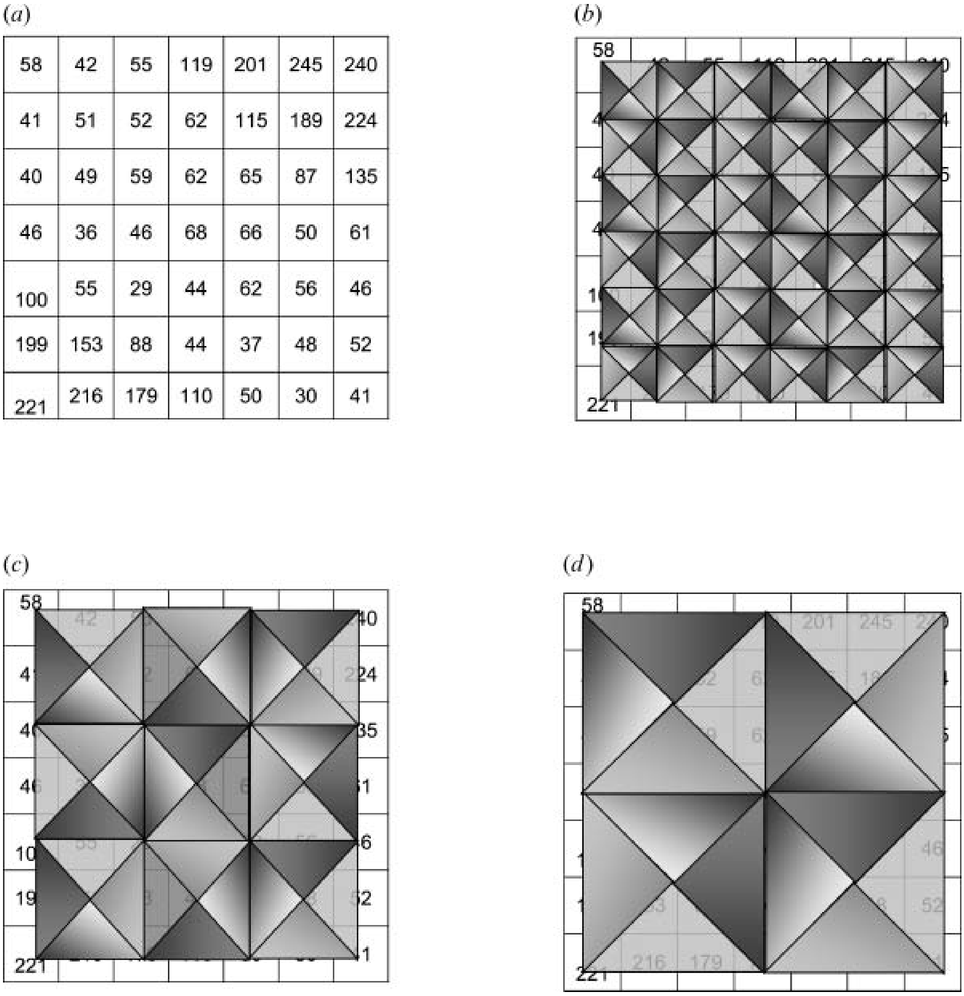


Figure 4. Computation of facet areas. (*a*) Example $7 \times 7$ pixel image; (*b*) Step 1 – $2 \times 2$ prisms; (*c*) Step 2 – $3 \times 3$ prisms; (*d*) Step 3 – $4 \times 4$ prisms.

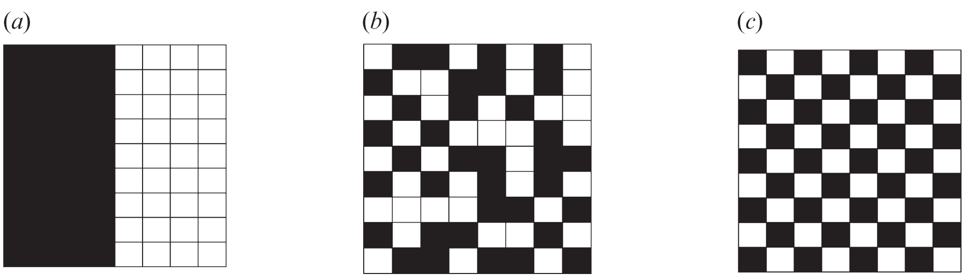


Figure 5. Example values of Moran's *I* index of spatial autocorrelation. (*a*) Clumped pattern $I \approx +1.0$; (*b*) Random pattern $I \approx 0.0$; (*c*) Dispersed pattern $I \approx -1.0$.

real number local variance, Moran's $I$ and fractal dimension values were converted to eight bit unsigned intergers using a linear stretch to make them compatible with the other multispectral bands.

In texture analysis, the size of the analysis window has an important impact on the ability to segment and classify an image (Marceau *et al*. 1990). For this investigation, several window sizes ranging from $7 \times 7$ pixels up to $29 \times 29$ pixels were tried. Although the local variance technique performed relatively well at small window sizes, the Moran's $I$ and fractal dimension measurements required larger windows to yield a stable result. The rook's case adjacent weighting in the Moran's $I$ algorithm limits accuracy for window sizes smaller than $11 \times 11$ pixels. The regression procedure in the fractal dimension algorithm also places a lower limit on the size of the moving window. Through experimentation with unsupervised clustering of the texture images, it was found that a $21 \times 21$ window size yielded images that most closely match the reference data land cover patterns. This window size was used in this analysis for all of the methods (although the local variance method performed slightly better at a $7 \times 7$ window size).

With an arithmetic increase in pixel size for each step, a $21 \times 21$ pixel moving window size allows ten computations of the log (prism area)/log (pixel size) expression per window, yielding a fairly stable regression line for computing fractal dimension. Although the edge effects are reduced using smaller window sizes, small windows have fewer points in the fractal dimension regression and less stable Moran's $I$ results, yielding noisy output images.

### 2.6 *Image classification*

Table 1 shows the land cover categories that were used in this analysis. These categories are based the USGS Anderson Level I land cover classification (Anderson *et al*. 1976), with the urban category subdivided into high and low intensity groups. The 8-bit local variance, fractal dimension, and Moran's $I$ images were added to the stack of visible and reflective infrared bands. Spectral signatures were derived for the five land cover categories using the training sites depicted in figure 6. The signatures included only the visible and reflective infrared bands in the case of the multispectral only classification. Each of the texture images were added in turn to the signatures for the multispectral + local variance, multispectral + fractal dimension, and multispectral + Moran's $I$ classifications.

Example panchromatic images from these training sites are shown in figure 7. The large commercial buildings and other extensive features in the high intensity urban category (figure 7(*a*)) led to a coarse texture, with individual objects often composed of several pixels. Low intensity urban areas (figure 7(*b*)) were complex collections of

Table 1. Land cover classification categories.

| Category | Land cover | Land use classes |
|---|---|---|
| 1 | Low intensity urban | Single/multifamily residential, mobile home parks |
| 2 | High intensity urban | Commercial, intensive institutional, industrial, transportation |
| 3 | Pasture/grassland | Agriculture, orchards, parks |
| 4 | Forest | Deciduous/evergreen/mixed forest, forested wetlands |
| 5 | Water | Lakes, ponds, rivers, reservoirs |

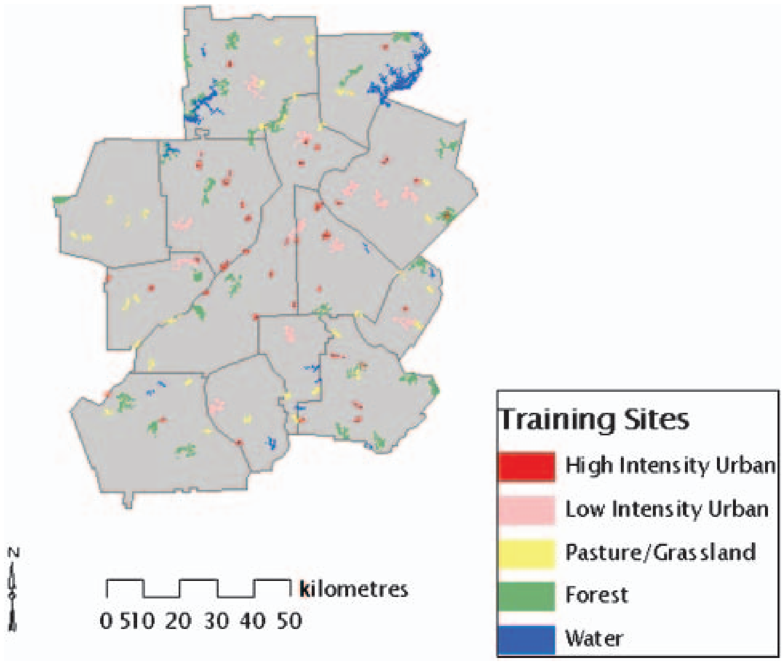


Figure 6. Training site locations.

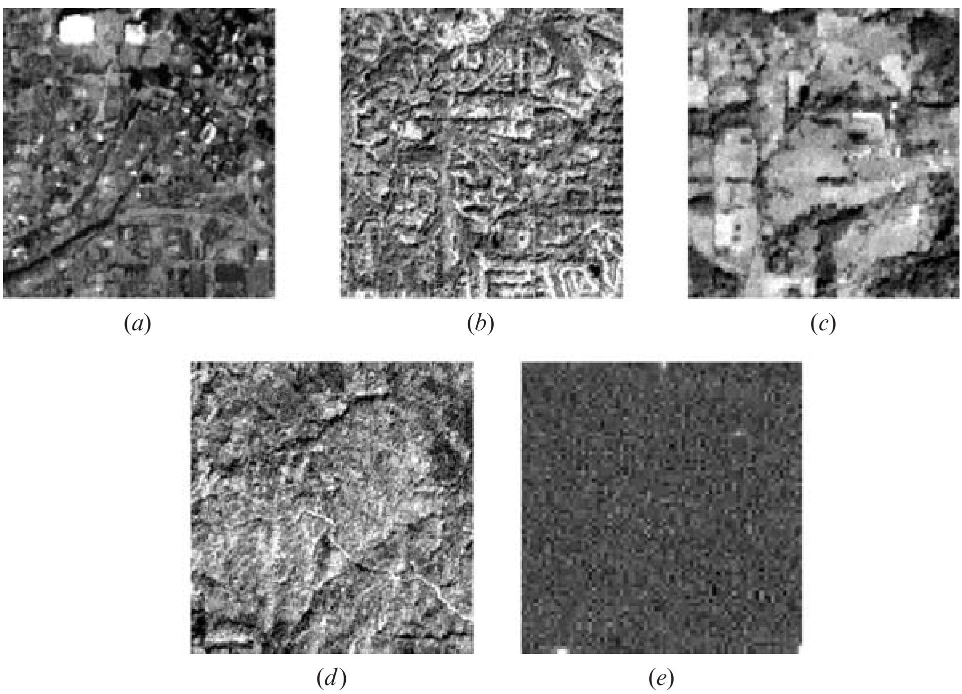


Figure 7. Example training site landcovers. (*a*) High intensity urban; (*b*) Low intensity urban; (*c*) Pasture/grassland; (*d*) Forest; (*e*) Water.

tree cover, street networks, and buildings. Pasture and grasslands (figure 7(*c*)) had a relatively smooth texture, often interspersed with shrubs and trees. Forests (figure 7(*d*)) were relatively uniform, but rough textured areas. Water areas (figure 7(*e*)) were smooth, dark, featureless areas with irregular outlines.

### 2.7 *Accuracy Assessment*

Reference data was acquired from the Atlanta Regional Commission (ARC) in the form of the LandPro99 GIS theme layer, which forms part of the Atlanta Regional Information System (ARIS)(ARC 2002). The geographic extent of this map (shown in figure 1) is a 13-county area which includes ARC's 10 counties, plus the adjacent counties of Forsyth, Paulding, and Coweta. This landuse/cover ArcView™ shapefile was created by on-screen photo-interpretation and digitizing of ortho-rectified aerial photography. The primary sources for this mapping effort were 1999 colour aerial photography that was obtained at a scale of 1:14,000 and digitized with a 1.22 metre pixel resolution, and 1999 colour infrared (CIR) US Geological Survey (USGS) digital orthophoto quarter quads (DOQQs) with one meter pixel resolution. Both sources of imagery were used to delineate landcover polygons, which were in turn aligned to the Georgia Department of Transportation digital line graph street centerlines. Polygons within the LandPro99 land cover map were recategorized and dissolved to correspond to the five class land cover classification scheme (table 1 and figure 2).

The minimum mapping unit standard for this database is generally five acres (2.02 hectares), with varying exceptions based on category and context. Smaller features in the intensive institutional (mostly elementary schools) category, commercial features, cemeteries, and reservoirs (impoundments) have been intentionally delineated in some cases throughout the region. This minimum mapping unit naturally leads to a mismatch of spatial scales between the 30 m square pixels in the classified images and the reference data. To partially overcome this, the accuracy assessment procedure in ERDAS Imagine™ included a $5 \times 5$ pixel majority filter around each accuracy point. If the pixels surrounding the accuracy assessment point have a more frequently occurring land cover category, the mode land cover in the $5 \times 5$ window was used for accuracy assessment purposes.

1000 randomly selected points in the 13-county Atlanta Regional Commission area were used to assess the accuracy of the ETM+ image using the LandPro99 (ARC 2002) GIS land cover map. This number of accuracy assessment points ensured that none of the land cover categories contained less than the recommended 50 points (Congalton and Green 1998).

## 3. Results and discussion

Images formed from local variance, Moran's *I,* and fractal dimension values were linearly stretched and rescaled to 8-bit unsigned integers to be compatible with the other spectral bands. Figure 8 shows the three texture images. In the local variance (figure 8(*a*)) image, Atlanta's urban core shows up as a lighter area indicating higher local variance values. The large lakes to the northeast and northwest of the city are visible as dark areas of low variance outlined by white lines indicating high areas of variance at the lake shores. Figure 8(*b*), the fractal dimension image shows the developed area of the city as darker areas of intermediate fractal dimension values. The lakes are clearly visible, and the forests and grasslands in the city hinterlands are

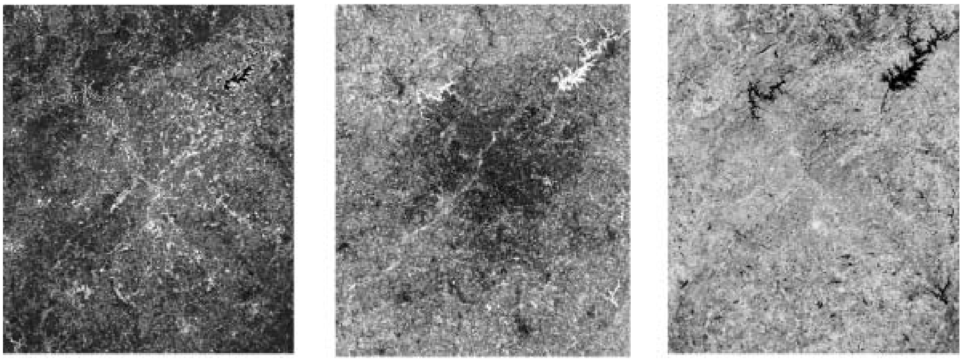

(a) (b) (c)

Figure 8. Texture images derived from ETM+ panchromatic image. (a) Local variance; (b) Fractal dimension; (c) Moran's I.

a complex mix of high and low fractal dimensions. The Moran's *I* image does not clearly delineate the city, and it appears to mainly highlight topography and shadows. The descriptive statistics of these images are shown in table 2. The narrow range of values in the Moran's *I* image meant that textures that appear quite different have roughly similar Moran's *I* values, thus limiting this technique's ability to distinguish between land covers.

Table 3 shows the results of the accuracy assessment of the four classified images. In the multispectral only classification (table 3*a*), the errors of omission (producer's accuracy) in the low intensity urban category were the major factor limiting overall accuracy. Less than 30% of the 249 low intensity urban accuracy points were classified correctly with most of the misidentification being in the forest category. Errors of commission (user's accuracy) for forest were therefore high, and the multispectral only classification also had some difficulty resolving forest from pasture/grassland.

Adding local variance to the multispectral bands improved the classification of the high intensity urban class (table 3*b*). This strategy also had the fewest number of errors of omission for the water category, although it also tended to incorrectly identify many other accuracy points as water. Water's smooth texture and uniformly low digital numbers in the multispectral bands led to the classification of dark, featureless areas as water. Although local variance also helped in the identification of low intensity urban areas, the producer's accuracy for this class was still less than 40%.

The highest overall percent correctly classified (PCC) and KHAT statistics were obtained by adding the fractal dimension band to the multispectral layers. Of particular note is the greatly improved producer's accuracy for the low intensity urban class. The fractal dimension algorithm was best able to integrate brightness values within the $21 \times 21$ moving window to separate low intensity urban areas from

Table 2. Descriptive statistics for computed texture layers.

| Layer | Mean | Standard deviation | Min | Max |
|---|---|---|---|---|
| Local variance | 39.8 | 37.76 | 0.18 | 1935.8 |
| Fractal dimension | 2.7 | 0.09 | 1.9 | 3.66 |
| Moran's I | 0.89 | 0.05 | 0.84 | 0.99 |

Table 3. Confusion matrices for supervised classification of multispectral bands with fractal layers.

| a. Multispectral only | Reference land cover | | | | | | | |
|---|---|---|---|---|---|---|---|---|
| Classified land cover | High intensity urban | Pasture | Water | Low intensity urban | Forest | Class. total | User's accuracy (%) | KHAT |
| High intensity urban | 118 | 4 | 1 | 10 | 5 | 138 | 85.51 | 0.828 |
| Pasture/grassland | 5 | 105 | 1 | 19 | 14 | 144 | 72.92 | 0.670 |
| Water | 2 | 1 | 72 | 6 | 2 | 83 | 86.75 | 0.855 |
| Low intenisty urban | 22 | 2 | 2 | 74 | 6 | 106 | 69.81 | 0.598 |
| Forest | 9 | 67 | 11 | 140 | 302 | 529 | 57.09 | 0.361 |
| Reference totals | 156 | 179 | 87 | 249 | 329 | 1000 | | |
| Producer's accuracy (%) | 75.64 | 58.66 | 82.76 | 29.72 | 91.79 | | | |
| | PCC | KHAT | | | | | | |
| | 67.10% | 0.558 | | | | | | |

| b. Local variance + multispectral | Reference land cover | | | | | | | |
|---|---|---|---|---|---|---|---|---|
| Classified land cover | High intensity urban | Pasture | Water | Low intensity urban | Forest | Class. total | User's accuracy (%) | KHAT |
| High intensity urban | 128 | 2 | 1 | 4 | 5 | 140 | 91.43 | 0.989 |
| Pasture/grassland | 10 | 130 | 4 | 14 | 17 | 175 | 74.29 | 0.687 |
| Water | 4 | 3 | 75 | 4 | 7 | 93 | 80.65 | 0.788 |
| Low intensity urban | 7 | 2 | 0 | 98 | 7 | 114 | 85.96 | 0.813 |
| Forest | 7 | 42 | 7 | 129 | 293 | 478 | 61.30 | 0.423 |
| Reference totals | 156 | 179 | 87 | 249 | 329 | 1000 | | |
| Producer's accuracy (%) | 82.05 | 72.63 | 86.21 | 39.36 | 89.06 | | | |
| | PCC | KHAT | | | | | | |
| | 72.40% | 0.634 | | | | | | |

forests. However, fractal dimension was not as effective at separating low from high intensity urban, thus leading to a lower user's accuracy for these classes as compared to the local variance method.

The Moran's *I* and multispectral method improved the overall PCC and KHAT statistics only slightly over the multispectral only method. This method was able to improve the producer's accuracy for pasture/grassland as compared to the multispectral only strategy, by reducing the number of points that were mididentified as forest.

Table 4 compares the estimates of total area in the 13-county Landpro99 region for each landcover type as represented in a rasterized version of Landpro99 and each of the classification schemes (multispectral only, multispectral + local variance, multispectral + fractal dimension, and multispectral + Moran's *I*). The closest estimate to these benchmark areas was obtained through the multispectral + fractal

| c. Fractal + multispectral | | Reference land cover | | | | | | |
|---|---|---|---|---|---|---|---|---|
| Classified land cover | High intensity urban | Pasture | Water | Low intensity urban | Forest | Class. total | User's accuracy (%) | KHAT |
| High intensity urban | 115 | 3 | 1 | 9 | 4 | 132 | 87.12 | 0.847 |
| Pasture/grassland | 7 | 112 | 3 | 14 | 15 | 151 | 74.17 | 0.685 |
| Water | 0 | 0 | 71 | 4 | 1 | 76 | 93.42 | 0.928 |
| Low intensity urban | 27 | 9 | 0 | 181 | 15 | 232 | 78.02 | 0.707 |
| Forest | 7 | 55 | 12 | 41 | 294 | 409 | 71.88 | 0.581 |
| Reference totals | 156 | 179 | 87 | 249 | 329 | 1000 | | |
| Producer's accuracy (%) | 73.72 | 62.57 | 81.61 | 72.69 | 89.36 | | | |
| | PCC | KHAT | | | | | | |
| | 77.30% | 0.699 | | | | | | |

| d. Moran's I + multispectral | | Reference land cover | | | | | | |
|---|---|---|---|---|---|---|---|---|
| Classified land cover | High intensity urban | Pasture | Water | Low intensity urban | Forest | Class. total | User's accuracy (%) | KHAT |
| High intensity urban | 117 | 2 | 1 | 9 | 3 | 132 | 88.64 | 0.865 |
| Pasture/grassland | 15 | 144 | 6 | 33 | 22 | 220 | 65.45 | 0.579 |
| Water | 1 | 0 | 72 | 6 | 1 | 80 | 90.00 | 0.891 |
| Low intensity urban | 17 | 2 | 2 | 66 | 8 | 95 | 69.47 | 0.594 |
| Forest | 6 | 31 | 6 | 135 | 295 | 473 | 62.37 | 0.439 |
| Reference totals | 156 | 179 | 87 | 249 | 329 | 1000 | | |
| Producer's accuracy (%) | 75.00 | 80.45 | 82.76 | 26.51 | 89.67 | | | |
| | PCC | KHAT | | | | | | |
| | 69.40% | 0.594 | | | | | | |

Table 4. Land cover areas (in square kilometres) for the LandPro99 map and classified images.

| Land cover | LandPro99 30 m raster | Multispectral only | Multispectral + local var. | Multispectral + fractal | Multispectral + Moran's I |
|---|---|---|---|---|---|
| High intensity urban | 1100.3 | 1016.1 | 1068.8 | 1028.0 | 1028.0 |
| Pasture | 1409.4 | 1609.7 | 1764.3 | 1492.1 | 2171.2 |
| Water | 175.2 | 349.1 | 403.5 | 291.6 | 320.5 |
| Low intensity urban | 3512.5 | 1764.3 | 1854.3 | 2920.2 | 1640.2 |
| Forest | 4245.3 | 5712.6 | 5360.8 | 4719.8 | 5291.9 |
| **Total** | **10442.7** | **10451.7** | **10451.7** | **10451.7** | **10451.7** |

dimension classification for all of the land cover classes except for high intensity urban, for which multispectral + local variance had the closest estimate. However, all of the areal estimates of land cover obtained from classified imagery underestimated the low and high intensity urban classes and overestimated the water, forest, and pasture/grassland areas.

The spectral signature of water is so different from the other land cover classes, that even a relatively small patch of water in a 30 m instantaneous field of view led the whole pixel to be classified as water in many cases. Since 290 of the 1084 lakes and reservoirs in the LandPro 99 land cover map are less than the 2.02 hectare (5 acre) minimum mapping unit for this data set, it is probable that the $5 \times 5$ majority window used in the accuracy assessment led to underestimations of the errors of commission and inflated the user's accuracies in table 3.

Small structures sometimes led to a parcel being categorized as low or high intensity urban in the LandPro99 map, even though a large part of the parcel was actually covered by grass or forest. This landcover vs landuse conundrum led to the systematic overestimation of vegetated land cover areas by the image classification techniques.

## 4. Conclusions and notes for further research

Texture measures such as local variance, fractal dimension and Moran's *I* can combine synergistically with traditional multispectral classification techniques to yield more accurate results. Adding fractal dimension information to the multispectral bands is particularly helpful in resolving low density residential areas from surrounding undeveloped forest and grasslands. The overall percentage of correctly classified points increased from 67.1% to 77.3% with the addition of fractal dimension, with most of the improvement occurring in the forest and low intensity urban classes. Local variance performed better than Moran's *I*, but relatively poor classification accuracy in the forest and low intensity urban landcover classes kept overall percent correctly classified and KHAT indices below that of the multispectral with fractal dimension strategy.

The results presented here show some promise, but much work remains in order to better utilize these indices of image complexity. Texture is very scale-dependent, and the size of the moving window combined with the resolution of the imagery plays a big part in determining what features are highlighted by these techniques. Texture also involves directionality—a key means for distinguishing between textures is the orientation of the pattern. In the future we hope to include anisotropy as a means of distinguishing land covers and we hope to explore the potential benefits of other texture measurement algorithms.

### Acknowledgements

This research is supported by a research grant from NASA Intelligent Systems research grant (NCC-2-1246). We also thank Chris Caird, Ernie Anderson, and Wei Zhao for their technical assistance.

### References

Anderson, J.R., Hardy, E.E., Roach, J.T. and Witmer, R.E., 1976, A land use and land cover classification system for use with remote sensor data. U.S. Geological Survey Professional Paper 964 (Washington, D.C.: U.S. Government Printing Office).

Atlanta Regional Commission (ARC), 2002, *Atlanta Regional Information System (ARIS)* (Atlanta, Georgia: Atlanta Regional Commission).

Batty, M. and Longley, P.A., 1994, *Fractal Cities: A Geometry of Form and Function* (London: Academic Press).

Carr, J.R. and Miranda, F.P., 1998, The semivariogram in comparison to the co-occurrence matrix for classification of image texture. *IEEE Transactions on Geoscience and Remote Sensing*, **36**, pp. 1945–1952.

Chen, C.C. and Chen, C.C., 1999, Filtering methods for texture discrimination. *Pattern Recognition Letters*, **20**, pp. 783–790.

Chen, Y.Q., Nixon, M.S. and Thomas, D.W., 1997, On texture classification. *International Journal of Systems Science*, **18**, pp. 763–783.

Clarke, K.C., 1986, Computation of the fractal dimension of topographic surfaces using the triangular prism surface area method. *Computers and Geosciences*, **12**, pp. 713–722.

Cliff, A.D. and Ord, J.K., 1973, *Spatial Autocorrelation* (London: Pion Limited).

Congalton, R.C. and Green, K., 1998, *Assessing the Accuracy of Remotely Sensed Data: Principles and Practices* (Boca Raton, FL: Lewis Publishers).

Goodchild, M.F., 1980, *Spatial Autocorrelation, Concepts and Techniques in Geography* (CATMOG), Series No. 47 (Norwich, UK: GeoBooks).

Haralick, R.M., Shanmugam, K. and Dinstein, I., 1973, Textural features for image classification. *IEEE Transactions on Systems, Man, and Cybernetics*, SMC-3, pp. 610–621.

Jaggi, S., Quattrochi, D.A. and Lam, N.S.-N., 1993, Implementation and operation of three fractal measurement algorithms for analysis of remote-sensing data. *Computers and Geosciences*, **19**, pp. 745–767.

Johnsson, K., 1994, Segment-based land-use classification from SPOT satellite data. *Photogrammetric Engineering and Remote Sensing*, **60**, pp. 47–53.

Karathanassi, V., Iossifidis, C.H. and Rokos, D., 2000, A texture-based classification method for classifying built areas according to their density. *International Journal of Remote Sensing*, **21**, pp. 1807–1823.

Kolankiewicz, L. and Beck, R., 2001, *Weighing Sprawl Factors in Large U.S. Cities* (Arlington, VA: NumbersUSA).

Lam, N.S.-N., Qiu, H.L., Quattrochi, D.A. and Emerson, C.W., 2002, An evaluation of fractal methods for characterizing image complexity. *Cartography and Geographic Information Science*, **29**, pp. 25–35.

Lam, N.S.-N., Quattrochi, D.A., Qiu, H.-L. and Zhao, W., 1998, Environmental assessment and monitoring with image characterization and modeling system using multiscale remote sensing data. *Applied Geographic Studies*, **2**, pp. 77–93.

Leica Geosystems, 2002, ERDAS Imagine Version 8.6. Atlanta, Georgia, USA.

Mandelbrot, B.B., 1983, *The Fractal Geometry of Nature* (New York: W.H. Freeman and Co.).

Marceau, D.J., Howarth, P.J., Dubois, J.M. and Gratton, D.J., 1990, Evaluation of the grey-level co-occurrence matrix method for land-cover classsification using SPOT imagery. *IEEE Transactions on Geoscience and Remote Sensing*, **28**, pp. 513–518.

Pentland, A.P., 1984, Fractal-based description of natural scenes. *IEEE Transactions on Pattern Analysis and Machine Intelligence*, **6**, pp. 661–674.

Quattrochi, D.A., Lam, N.S.N., Qiu, H. and Zhao, W., 1997, Image Characterization and Modeling System (ICAMS): A geographic information system for the characterization and modeling of multiscale remote sensing data. In *Scale in Remote Sensing and GIS*, D.A. Quattrochi and M.F. Goodchild (Eds), pp. 295–308 (Boca Raton, FL: CRC Press).

Sali, E. and Wolfson, H., 1992, Texture classification in aerial photographs and satellite data. *International Journal of Remote Sensing*, **13**, pp. 3395–3408.

Woodcock, C.E. and Strahler, A.H., 1987, The factor of scale in remote sensing. *Remote Sensing of Environment*, **21**, pp. 311–322.

Zhang, Y., 1999, Optimisation of building detection in satellite images by combining multispectral classification and texture filtering. *ISPRS Journal of Photogrammetry and Remote Sensing*, **54**, pp. 50–60.

Zhao, W., 2001, *Multiscale analysis for characterization of remotely sensed images*, Ph.D. Dissertation, Louisiana State University, December 2001.